www.nature.com/aps

Acta Pharmacologica Sinica

ARTICLE

Chalcone derivatives ameliorate lipopolysaccharide-induced acute lung injury and inflammation by targeting MD2

Ya-li Zhang[1,2,3], Wen-xin Zhang[1,4], Jue-qian Yan[1], Ye-lin Tang[1], Wen-jing Jia[1,4], Zheng-wei Xu[1], Ming-jiang Xu[1], Nipon Chattipakorn[5], Yi Wang[1], Jian-peng Feng[1], Zhi-guo Liu[1,4] and Guang Liang[1,3,6]

Acute lung injury (ALI) and its severe form acute respiratory distress syndrome (ARDS) are known as the common causes of respiratory failure in critically ill patients. Myeloid differentiation 2 (MD2), a co-receptor of toll like receptor 4 (TLR4), plays an important role in LPS-induced ALI in mice. Since MD2 inhibition by pharmacological inhibitors or gene knockout significantly attenuates ALI in animal models, MD2 has become an attractive target for the treatment of ALI. In this study we identified two chalcone-derived compounds, **7w** and **7x**, as new MD2 inhibitors, and investigated the therapeutic effects of **7x** and **7w** in LPS-induced ALI mouse model. In molecular docking analysis we found that **7w** and **7x**, formed pi-pi stacking interactions with Phe^{151} residue of the MD2 protein. The direct binding was confirmed by surface plasmon resonance analysis (with KD value of 96.2 and 31.2 μM, respectively) and by bis-ANS displacement assay. **7w** and **7x** (2.5, 10 μM) also dose-dependently inhibited the interaction between lipopolysaccharide (LPS) and rhMD2 and LPS-MD2-TLR4 complex formation. In mouse peritoneal macrophages, **7w** and **7x** (1.25−10 μM) dose-dependently inhibited LPS-induced inflammatory responses, MAPKs (JNK, ERK and P38) phosphorylation as well as NF-κB activation. Finally, oral administration of **7w** or **7x** (10 mg·kg^{-1} per day, for 7 days prior LPS challenge) in ALI mouse model significantly alleviated LPS-induced lung injury, pulmonary edema, lung permeability, inflammatory cells infiltration, inflammatory cytokines expression and MD2/TLR4 complex formation. In summary, we identify **7w** and **7x** as new MD2 inhibitors to inhibit inflammatory response both in vitro and in vivo, proving the therapeutic potential of **7w** and **7x** for ALI and inflammatory diseases.

Keywords: acute lung injury; myeloid differentiation 2; inflammation; chalcone derivatives; lipopolysaccharide; mouse peritoneal macrophages

Acta Pharmacologica Sinica (2022) 43:76–85; https://doi.org/10.1038/s41401-021-00764-8

INTRODUCTION

Acute lung injury (ALI) and the severe form of acute respiratory distress syndrome (ARDS) are a class of complicated and life-threatening diseases characterized by severe inflammation and increased lung permeability leading to alveolar edema, hypoxemia and organ failure [1, 2]. A variety of different factors, such as endotoxemia, mechanical ventilation, trauma, and shock, can cause ALI/ARDS in either a direct or indirect manner [3–6]. Although great progress has been achieved so far in understanding the pathogenesis of ALI, the mortality of ALI remains high [7, 8]. Currently, there is still no clinically effective treatment for ALI.

Lipopolysaccharide (LPS), as the major cell wall component of Gram-negative bacteria, is capable to induce overexpression of many inflammatory mediators and cause impairment of multiple organs [9, 10]. The LPS-induced animal ALI model reflects several key pathologic processes of ALI/ARDS and has been established to explore the underlying mechanism and potential therapies of ALI [11]. Myeloid differentiation 2 (MD2), a co-receptor of toll like receptor 4 (TLR4), plays a pivotal role in the recognition of LPS by TLR4 [12]. The interaction between LPS and TLR4/MD2 induces homotypic dimerization to form $(LPS\text{-}MD2\text{-}TLR4)_2$ multimer, which leads to the recruitment of myeloid differentiation factor 88 and the subsequent activation of intracellular signaling pathways (MAPKs and NF-κB), thereby leading to the production of pro-inflammatory cytokines [13, 14]. MD2 inhibition caused by either pharmacological inhibitors or gene knockout significantly attenuates ALI in animal models, which proves MD2 as an attractive target for the treatment of ALI [15, 16].

Up to now, there have been several chalcone derivatives identified as MD2 specific inhibitors, including xanthohumol, L2H21, L40H37, and L6H21 (Fig. 1a) [17–20]. These chalcone derivatives share the same skeleton of *(E)*-4-phenylbut-3-en-2-one and exhibit anti-inflammatory activities in LPS-induced ALI and sepsis models. Recently, we synthesized a series of chalcone derivatives with 2-benzylidene-1-indanone structure, which possess

[1]Chemical Biology Research Center, School of Pharmaceutical Sciences, Wenzhou Medical University, Wenzhou 325035, China; [2]Key Laboratory of Molecular Pharmacology and Drug Evaluation (Yantai University), Ministry of Education, Yantai University, Yantai 264005, China; [3]School of Pharmaceutical Sciences, Hangzhou Medical College, Hangzhou 311399, China; [4]Zhuji Biomedicine Institute, School of Pharmaceutical Sciences, Wenzhou Medical University, Zhuji 311800, China; [5]Cardiac Electrophysiology Research and Training Center, Faculty of Medicine, Chiang Mai University, Chiang Mai 50200, Thailand and [6]Wenzhou Institute, University of Chinese Academy of Sciences, Wenzhou 325001, China

Correspondence: Ya-li Zhang (ya-li000@163.com) or Zhi-guo Liu (lzgcnu@163.com) or Guang Liang (wzmcliangguang@163.com)

These authors contributed equally: Ya-li Zhang, Wen-xin Zhang, Jue-qian Yan

Received: 12 January 2021 Accepted: 10 August 2021
Published online: 3 September 2021

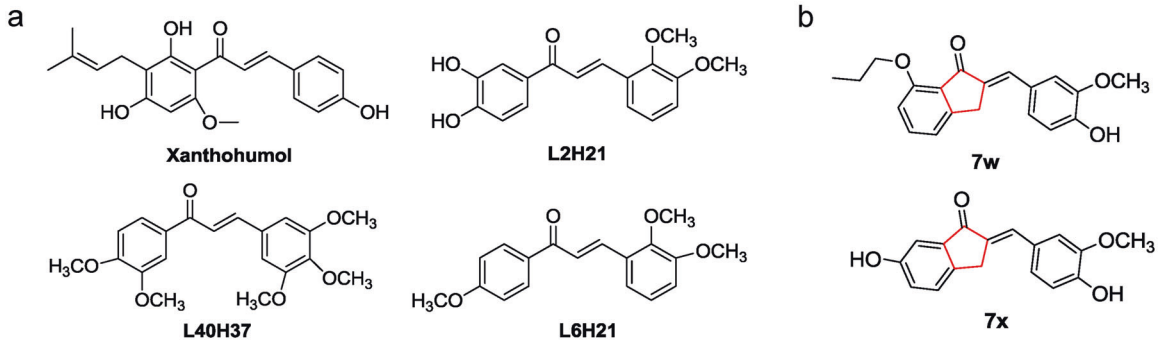

Fig. 1 The chemical structures of MD2 inhibitors. a Previous reported MD2 inhibitors. **b** The chemical structures of **7w** and **7x**.

stable chemical structure and also show anti-inflammatory effects in vitro [21]. Among them, *(E)*-6-hydroxy-2-(4-hydroxy-3-methoxybenzylidene)-2,3-dihydro-*1H*-inden-1-one (**7x**) and *(E)*-2-(4-hydroxy-3-methoxybenzylidene)-7-propoxy-2,3-dihydro-*1H*-inden-1-one (**7w**) showed the greatest anti-inflammatory activities in cultured macrophages (Fig. 1b). However, the underlying mechanism accounting for their anti-inflammatory activities remains unknown.

Due to the similarity in chemical structures of 2-benzylidene-1-indanone derivatives and *(E)*-4-phenylbut-3-en-2-one derivatives (Fig. 1b), we hypothesized that the anti-inflammatory properties of **7x** and **7w** may be mediated by direct interaction with MD2 protein. In this study, we identified the direct interaction of **7x** and **7w** with MD2, and the therapeutic effects of **7x** and **7w** in LPS-induced ALI were further demonstrated through targeting MD2 and disrupting LPS-MD2-TLR4 complex formation.

MATERIALS AND METHODS

Reagents

LPS was purchased from Sigma-Aldrich (St. Louis, MO, USA). Recombinant human MD2 (rhMD2) and rhTLR4 proteins were purchased from R&D (Minneapolis, MN, USA). Antibodies against P38, p-P38, JNK, p-JNK, P65, GAPDH, and IκBα were from Cell Signaling Technology (Danvers, MA, USA); antibodies against F4/80, ERK, and p-ERK were from Santa Cruz Biotechnology (Dallas, TX, USA); antibodies against Lamin B, MD2, and TLR4 were from Abcam (Cambridge, UK); antibodies against HA and FLAG were from Sigma-Aldrich (St. Louis, MO, USA). Compounds **7w** and **7x** were synthesized in our lab and the structures were confirmed using MS and ^{1}H NMR [21]. For in vivo studies, **7w** and **7x** were dissolved in 0.5% CMC-Na in water solution. For in vitro studies, **7w** and **7x** were dissolved in dimethyl sulfoxide (DMSO), and the same amount of DMSO was used as the vehicle control.

Cell culture

Human kidney 293T cells were obtained from National Collection of Authenticated Cell Cultures (Shanghai, China). Mouse J774a.1 macrophages were purchased from Procell (Wuhan, China). The cells were cultured in DMEM medium (Gibco, Eggenstein, Germany) supplemented with 10% heat inactivated fetal bovine serum (FBS, Hyclone, Logan, UT, USA), 100 U/mL penicillin and 100 mg/mL streptomycin (NCM Biotech, Suzhou, China).

Mouse peritoneal macrophages (MPMs) were isolated from C57BL/6 mice after intraperitoneally (i.p.) injected with 3 mL 6% starch broth solution for 2 days. MPMs were collected by washing the peritoneal cavity with 8 mL RPMI-1640 medium (Gibco, Eggenstein, Germany) per mouse. Cell suspension was centrifuged. The cell pellet was resuspended in RPMI-1640 medium containing 10% FBS, and then cultured at 37 °C with 5% CO_2. The non-adherent cells were washed out with medium after 4 h, and the adherent cells were used in the experiments.

Animal studies

All animal studies and experimental procedures were approved by Wenzhou Medical University Animal Policy and Welfare Committee (Approval No. wydw2016-0124) in according to the National Institutes of Health (USA) guidelines. Male C57BL/6 mice at 8-week-old were obtained from the Animal Center of Wenzhou Medical University (Wenzhou, China). Mice were allowed to acclimate for at least 7 days before subjected to the study.

ALI model. Mice were randomly divided into four groups ($n = 8$ per group), i.e., control group (CON), ALI group (intratracheal instillation of LPS at 5 mg/kg), ALI + **7w** treatment group (LPS + **7w**), ALI + **7x** treatment group (LPS + **7x**). For preventive study: vehicle control (0.5% CMC-Na), **7w** and **7x** (both at 10 mg· kg^{-1} per day) were orally administered for 7 days before mice were challenged by intratracheal instillation of LPS (5 mg/kg in 0.9% saline). Mice in CON group were orally administered 0.5% CMC-Na solution for 7 days before intratracheal injected with 0.9% saline. For therapeutic study: mice were intragastricly administered 10 mg/kg **7w** or **7x** one hour after intratracheal instillation of 5 mg/kg LPS. Mice in CON group were orally administered 0.5% CMC-Na solution 1 h after intratracheal injection with 0.9% saline. Mice were euthanized with chloral hydrate 6 h after LPS challenge. Broncho alveolar lavage fluid (BALF) and blood samples were collected. Lung tissues were snap frozen with liquid nitrogen and stored at −80 °C for analyses.

Toxicity study. Twenty-four male C57BL/6 mice were divided into three groups ($n = 5$ per group), i.e., control group (CON), **7w** treatment group (**7w** 10 mg/kg), and **7x** treatment group (**7x** 10 mg/kg). Mice in **7w** and **7x** treatment group were orally administered 10 mg/kg **7w** and **7x**, respectively, for 7 days. Mice in CON group were administered the vehicle control (0.5% CMC-Na solution) for 7 days. Blood samples and lung tissues were collected on the eighth day.

Measurement of alanine aminotransferase (ALT), aspartate aminotransferase (AST), and lactic dehydrogenase (LDH)

The levels of ALT, AST, and LDH were calculated using ALT, AST, and LDH detection kits (Nanjing Jiancheng Bioengineering Institute, Nanjing, China) according to the manufacturer's instructions.

TNF-α and IL-6 levels determination

TNF-α and IL-6 content in culture medium or animal samples were determined with ELISA kits from eBioscience (San Diego, CA, USA) according to the manufacturer's instructions. The amount of TNF-α or IL-6 was normalized to the protein concentration of lysates.

Real-time quantitative PCR

Total RNA was isolated from the cells or lung tissues (10–20 mg) using the TRIzol reagent (Invitrogen, Carlsbad, CA, USA). Reverse

transcription and qPCR were carried out using a two-step M-MLV Platinum SYBR Green qPCR SuperMix-UDG kit (Invitrogen, Carlsbad, CA, USA). Eppendorf Mastercycler ep realplex detection system (Eppendorf, Hamburg, Germany) was used for qPCR analysis. All primers were synthesized by Invitrogen (Shanghai, China). Mouse TNF-α forward primer, 5′-CCCTCACACTCAGATCATCTTCT-3′, mouse TNF-α reverse primer, 5′-GCTACGACGTGGGCTACAG-3′; Mouse IL-6 forward primer, 5′-GAGGATACCACTCCCAACAGACC-3′, mouse IL-6 reverse primer, 5′-AAGTGCATCATCGTTGTTCATACA-3′; Mouse ICAM-1 forward primer, 5′-GCCTTGGTAGAGGTGACTGAG-3′, mouse ICAM-1 reverse primer, 5′-GACCGGAGCTGAAAAGTTGTA-3′; Mouse VCAM-1 forward primer, 5′-TGCCGAGCTAAATTACACATTG-3′, mouse VCAM-1 reverse primer, 5′-CCTTGTGGAGGGATGTACAGA-3′; Mouse β-actin forward primer, 5′-CCGTGAAAAGATGACCCAGA-3′, mouse β-actin reverse primer, 5′-TACGACCAGAGGCATACAG-3′. Gene expression levels were relative to the corresponding β-actin expression.

Western blotting and immunoprecipitation

Protein concentrations of cell or tissue lysate were determined with Bradford assay (Bio-Rad Laboratories, Hercules, CA, USA). After being boiled in loading buffer for 10 min, samples were subjected to 10% SDS-PAGE and transferred onto a PVDF membrane (Bio-Rad Laboratories, Hercules, CA, USA). After being blocked in blocking buffer (5% milk in tris-buffered saline containing 0.05% Tween 20, TBST) for 1.5 h at room temperature, membranes were incubated with the primary antibodies at 4 °C overnight. Membranes were washed in TBST and incubated with HRP-conjugated secondary antibody for 1 h at room temperature. Blots were visualized using enhanced chemiluminescence reagents (Bio-Rad Laboratories, Hercules, CA, USA). The density of the immunoreactive bands was analyzed using ImageJ software (NIH, Bethesda, MD, USA).

For immunoprecipitation assay, cell or tissue lysates were prepared and incubated with anti-TLR4 antibody at 4 °C overnight. The immune complexes were precipitated with protein A + G agarose, and the precipitates were washed five times with ice-cold PBS. After being boiled in loading buffer, the samples were subjected to Western blot analysis.

TLR4 homodimerization analysis

The effects of **7w** and **7x** on TLR4 homodimerization was detected by immunoprecipitation. Human kidney 293T cells were co-transfected with HA-TLR4 (2 μg) and FLAG-TLR4 (2 μg) plasmids using Lipofectamine 2000 reagent according to the manufacturer's instructions. After 22 h, medium was replaced with fresh medium and the cells were incubated with 10 μM **7w** or **7x** for 30 min, followed by 0.5 μg/mL LPS for 15 min. Immunoprecipitation assay was conducted with anti-HA and anti-FLAG antibodies.

BALF analysis

BALF was centrifuged at 3000 r/min for 10 min at 4 °C. The supernatant was immediately stored at −80 °C. The cell pellet was resuspended in 50 μL saline. Total cells were counted using Count Star (Shanghai, China), and neutrophils were counted after Wright-Gimesa staining (Nanjing Jiancheng Bioengineering Institute). Then, the number of neutrophils was determined via counting 200 cells on a smear prepared through Wright-Giemsa staining (Nanjing Jiancheng Bioengineering Institute).

Ratio of wet/dry lung weight

The middle lobe of right lung was excised and weighted, and then the lung tissue was dried at 65 °C in a thermostatically controlled oven for 72 h and weighed. The lung wet/dry (W/D) weight ratio was calculated to assess the pulmonary edema.

Histopathology and immunohistochemistry analyses

Lung tissue samples were fixed in 4% paraformaldehyde and embedded in paraffin. Tissue sections (5 μm) were dehydrated and subjected to hematoxylin and eosin (H&E) or immunohistochemical staining. Briefly, rehydrated tissue sections were treated with 3% H_2O_2 for 30 min. After blocked with 1% BSA for 30 min, tissue sections were incubated with primary antibodies (anti-LY-6G and anti-F4/80) at 4 °C overnight. HRP conjugated secondary antibody and DAB were used for color development. The percentage of positive staining was measured by ImageJ software (NIH, Bethesda, MD, USA).

Lung injury score

Lung impairment was assessed by lung injury score ranging from 0 (normal) to 4 (severe) in four categories: neutrophil infiltration, interstitial inflammation, edema, and congestion. Each category was graded on a 0–4 points scale, with 0 indicating no injury, 1 indicating injury up to 25% of the field, 2 indicating injury up to 50% of the field, 3 indicating injury up to 75% of the field, and 4 indicating diffuse injury. Grading was performed by a pathologist blinded to the study. The individual scores for each category were factored into the lung injury score. For each animal, the lung injury score was calculated as the sum of five sections.

NF-κB P65 translocation analyses

MPMs were pretreated with **7w** or **7x** (10 μM) for 30 min, and then stimulated with LPS (0.5 μg/mL) for 45 min. Proteins from the nuclear and cytoplasm fractions were prepared using a kit from Beyotime (Shanghai, China) according to the manufacturer's instructions, and then subjected to Western blot for the detection of P65. The translocation of P65 was confirmed using immunofluorescence staining with anti-P65 antibody and PE conjugated secondary antibody. The cells were counterstained with DAPI and viewed by Nikon fluorescence microscope (Nikon, Tokyo, Japan).

Surface plasmon resonance (SPR) analyses

The binding affinity of compounds to MD2 protein was detected using ProteOn XPR36 Protein Interaction Array system (Bio-Rad Laboratories) with a GLH sensor chip (Bio-Rad Laboratories, #1765013). Briefly, MD2 protein (in acetate acid buffer) was immobilized on the sensor after activated by 40 mM EDC and 10 mM sNHS in water solution. Compounds **7w** and **7x** at different concentrations were dissolved in running buffer with 5% DMSO and injected simultaneously at a flow rate of 30 μL/min for 120 s of association phase, followed with 200 s of dissociation phase at 25 °C. KD values were calculated by global fitting of the kinetic data using 1:1 Langmuir binding model.

Bis-ANS displacement assay

1,1′-Bis(anilino)-4,4′-bis(naphthalene)-8,8′-disulfonate (bis-ANS, Life Technologies, Carlsbad, CA, USA, 1 μM) and rhMD2 (5 nM) were mixed in PBS (pH 7.4) to reach stable fluorescence intensity under excitation at 385 nm. **7w** and **7x** at different concentrations were then added. Relative fluorescence units emitted at 430–570 nm were measured by SpectraMax M5 (MD, California, USA) at 25 °C in 1 cm path-length quartz cuvettes.

LPS displacement assay

The binding of LPS to rhMD2 was determined by cell-free ELISA. The 96-well plates were coated with human MD2 antibody in 10 mM Tris-HCl buffer (pH 7.5) at 4 °C overnight. Plates were blocked with 3% BSA at room temperature for 1.5 h. RhMD2 was added at 4 μg/mL in 10 mM Tris-HCl buffer (pH 7.5) and incubated at room temperature for 1.5 h. Biotin-labeled LPS was then added with or without **7w** or **7x** and incubated at room temperature for 1 h. Streptavidin-conjugated HRP was added and incubated at room temperature for 1 h. TMB was added for color development.

The reaction was stopped with H_2SO_4 solution and *OD* values were measured at 450 nm.

Molecular docking of 7w and 7x to MD2

The molecular interactions were evaluated by a docking simulation study using AutoDock version 4.2.6. The crystal structure of human MD2-lipid IVa complex (PDB: 2E59) was obtained from Protein Data Bank for the docking simulation. The AutoDockTools version 1.5.6 package was applied to generate the docking input files and the docking results were analyzed. A 60 points × 60 points × 60 points grid box with a spacing of 0.375 Å between the grid points was implemented. The affinity maps of MD2 were calculated by AutoGrid. One hundred Lamarckian Genetic Algorithm runs with default parameter settings were processed. The hydrogen bonds and bond lengths within the interactions of complex protein-ligand conformations were analyzed.

Statistical analysis

All data represented at least three independent experiments and were expressed as mean ± SEM. All statistical analyses were performed using GraphPad Pro Prism 8.0 (GraphPad, San Diego, CA, USA). One-way ANOVA, followed by Dunn's *post hoc* test, was used when comparing multiple independent groups. $P < 0.05$ was considered statistically significant difference between groups.

RESULTS

Compounds 7w and 7x directly bind to MD2 and inhibit LPS-MD2-TLR4 complex formation

In order to identify the potential binding of **7w** and **7x** to MD2, **7w** and **7x** were docked to the crystal structure of the MD2 protein (PDB: 3FXI) using molecular docking software. As shown in Fig. 2a, b, compounds **7w** and **7x** fitted into the hydrophobic pocket of MD2 and were involved in pi-pi stacking interactions with Phe^{151} residue of the MD2 protein with a docking score of −8.1 and −7.8 kcal/mol, respectively.

Then, SPR assay was conducted to confirm the direct binding of compounds **7w** and **7x** to rhMD2. Both **7w** and **7x** interacted directly with rhMD2 protein with a KD value of 96.2 and 31.2 μM, respectively (Fig. 2c, d). However, no interaction signal was detected between **7w** and rhTLR4 protein (Supplementary Fig. S1a). Although our data found that **7x** also interacted rhTLR4 with a KD value of 133 μM, indicating a weak affinity of **7x** binding to TLR4 (Supplementary Fig. S1b), **7x** remains a selective MD2 inhibitor. These interactions were further confirmed with a bis-ANS displacement assay. Elevated florescence signals were observed after MD2 and bis-ANS incubation, which were inhibited by the presence of **7w** or **7x** (at 5 and 10 μM) (Fig. 2e, f). An ELISA-based LPS displacement assay showed that **7w** and **7x** competitively inhibited the interaction between bio-LPS and rhMD2 (Fig. 2g). More importantly, pretreatment with **7w** and **7x** obviously inhibited LPS-induced MD2/TLR4 complex formation in MPMs and TLR4 dimerization in HEK293 cells (Fig. 2h, i). These results suggest that compounds **7w** and **7x** directly bind to MD2 and inhibit LPS-MD2-TLR4 complex formation.

Compounds 7w and 7x inhibit LPS-induced inflammation in a dose-dependent manner

To explore the functional block of LPS-TLR4 signaling by **7w** and **7x**, J774a.1 macrophages were pretreated with **7w** or **7x** (1.25, 2.5, 5, and 10 μM) for 30 min and then treated with LPS (0.5 μg/mL) for 24 h. The LPS-induced releases of TNF-α and IL-6 in the culture medium were dose-dependently inhibited by **7w** and **7x**, whose corresponding IC_{50} values were 1.41 and 0.99 μM for TNF-α inhibition, and 1.05 and 2.12 μM for IL-6 inhibition (Fig. 3a, b). RT-qPCR analysis showed that the LPS-increased mRNA levels of TNF-α, IL-6, VCAM-1, and ICAM-1 were reduced by pretreatment with **7w** and **7x** at 5 and 10 μM, respectively (Fig. 3c, d). These results indicate that **7w** and **7x** dose-dependently inhibited the expression of LPS-induced inflammatory cytokines in macrophages.

Compounds 7w and 7x inhibit LPS-induced activation of MAPKs and NF-κB

Further investigation was conducted to evaluate the effects of **7w** and **7x** against LPS/TLR4 downstream signaling MAPKs and NF-κB activation. LPS significantly increased the phosphorylation of JNK, ERK, and P38 in MPMs, which were decreased by pretreatment of **7w** and **7x** (10 μM) (Fig. 4a). Similarly, LPS-activated NF-κB signaling, illustrated by decreased IκBα level, reduced cytoplasmic P65, and increased nuclear P65 levels, was markedly suppressed by the pretreatment of **7w** and **7x** (Fig. 4b). The LPS-induced translocation of P65 from cytoplasm to nucleus was substantiated by the immunofluorescence staining in MPMs blocked by **7w** and **7x** (Fig. 4c). These results suggest a significant inhibitory effect on LPS-TLR4 signaling pathway by **7w** and **7x**.

7w and 7x attenuate LPS-induced ALI in mice by targeting MD2

Since **7w** and **7x** exhibited significant inhibitory effect on LPS-MD2-TLR4 pro-inflammatory signaling in vitro, the effects of **7w** and **7x** on lung impairment were examined in mice. Firstly, the toxic effects of compounds **7w** and **7x** were evaluated in vivo. The administration of 10 mg/kg **7w** and **7x** for 7 consecutive days failed to induce phenotypic changes (body weight and behaviors) in mice and pathological change in the lung tissues (Supplementary Fig. S2a). Also, **7w** and **7x** did not affect the function of the livers, evidenced by the serum ALT, AST, and LDH levels (Supplementary Fig. S2b–d). The intratracheal instillation of LPS was used to construct the mouse model of ALI. According to H&E staining, LPS challenge induced obviously inflammatory cell infiltration and pulmonary edema, which was significantly improved by the pretreatment with **7w** and **7x** (Fig. 5a). These beneficial effects of **7w** and **7x** in the ALI model were indicated by the improvement of the lung injury scores (Fig. 5b), lung W/D weight ratio (Fig. 5c) and the total protein concentration in BALF (Fig. 5d). The reduction in the number of total cells (Fig. 5e) and neutrophils in BALF (Fig. 5f) evidenced the therapeutic effect of **7w** and **7x** in the ALI model by hindering the infiltration of inflammatory cell into the lung. The anti-inflammatory effects of **7w** and **7x** were further confirmed with the reduced positive staining against F4/80 (Fig. 5g, h) and Ly-6G (Fig. 5i, j) in the LPS-challenged mouse lungs.

Consistent with the in vitro results, the increased levels of TNF-α and IL-6 in both BALF (Fig. 6a, b) and sera (Fig. 6c, d) were significantly ameliorated with the **7w** and **7x** treatments in the ALI model. Similarly, the increase in transcript levels of pro-inflammatory cytokines TNF-α, IL-6, VCAM-1, and ICAM-1 in lung tissues was reduced by the treatment with **7w** and **7x** (Fig. 6e–h). Finally, immunoprecipitation assays revealed the increased MD2-TLR4 association in the lung tissues of LPS-challenged mice (Fig. 6i, j), and **7w** or **7x** treatment significantly reduced this MD2-TLR4 interaction. Taken together, these results suggest that **7w** or **7x** pretreatment improves pulmonary inflammation and edema in LPS-induced ALI model, which is potentially through disrupting LPS-induced MD2-TLR4 interaction.

Generally, drugs should be administered after the initiation of lung injury. We also evaluated the therapeutic effects of **7w** and **7x** in mice with LPS-induced ALI. Similar to the pre-administration experiment, our data showed that **7w** and **7x** significantly reduced the LPS-induced pathological injury of lung tissue (Fig. 7a, b), pulmonary edema (Fig. 7c), infiltration of inflammatory cells in BALF (Fig. 7d), and overproduced inflammatory cytokines IL-6 and TNF-α levels in BALF (Fig. 7e, f). These results prove that **7w** and **7x** are effective both in the prevention and therapy against LPS-induced ALI in mice.

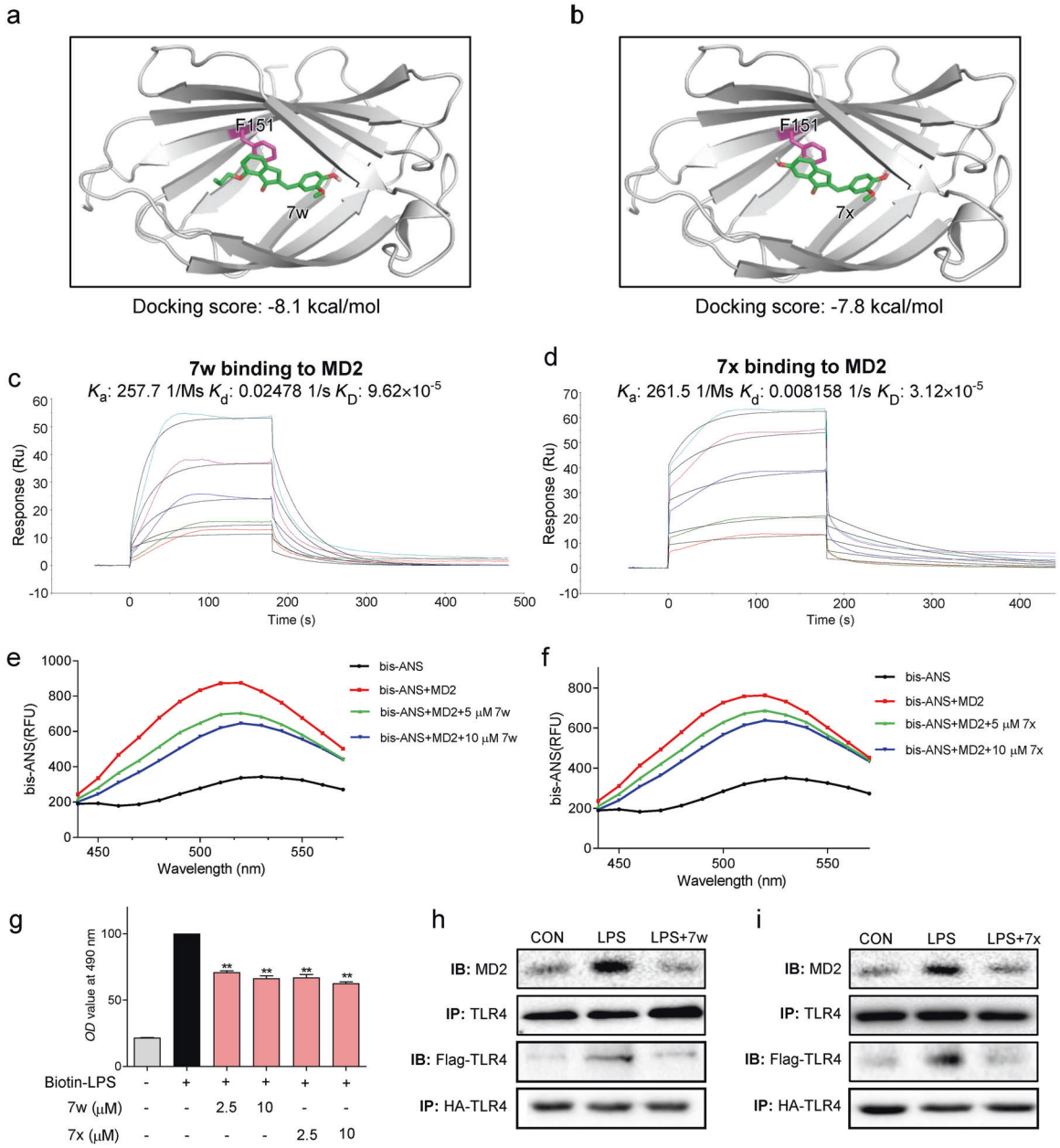

Fig. 2 7w and 7x are identified as new MD2 inhibitors. a, **b** Molecular dockings of **7w** and **7x** with rhMD2 (PDB: 2E56) were analyzed with the Tripos molecular modeling software. **c**, **d** The direct interactions of **7w** and **7x** with rhMD2 were shown by SPR assay. K_a binding constant, K_d dissociation constant, K_D equilibrium dissociation constant. **e**, **f** The effects of **7w** (5 and 10 μM) and **7x** (5 and 10 μM) on binding fluorescent bis-ANS (5 μM) to rhMD2. **g** As determined by ELISA, **7w** and **7x** dose-dependently inhibited the binding of biotin-LPS to rhMD2. **h**, **i** MPMs were pretreated with **7w** or **7x** at 10 μM for 30 min and then exposed to LPS for 15 min. The complex of MD2-TLR4 were detected by immunoprecipitation (upper two panels). 293T cells were co-transfected with HA-TLR4 and Flag-TLR4 plasmids. Then, cells were treated with LPS for 15 min with **7w** or **7x** at 10 μM. Cell extracts were co-immunoprecipitated and were detected by anti-Flag and anti-HA antibodies (lower two panels).

DISCUSSION

In this study, **7w** and **7x** were demonstrated to be capable of directly binding to MD2 and disrupt LPS-MD2-TLR4 complex formation. According to the in vitro results, **7w** and **7x** obviously inhibited the expression of LPS-induced inflammatory cytokines and the activation of MAPKs and NF-κB signaling pathways. Meanwhile, **7w** and **7x** treatment mitigated LPS-induced ALI in mice by reducing the inflammatory response accompanied with reduced MD2-TLR4 interaction.

Neutrophil infiltration into the lung was the hall-marker and a fundamental feature of ALI [22]. The number of neutrophils in BALF is correlated with the severity of disease in ARDS patients, and neutrophil depletion can reduce the severity of ARDS in mice [23, 24]. Thus, targeting neutrophil recruitment and activation and promoting neutrophil apoptosis are regarded as the potential approaches to treat ALI [9, 25]. In this study, the administration of **7w** and **7x** significantly inhibited LPS-induced neutrophil infiltration in both BALF and lung tissues. Meanwhile, the LPS-induced gene expression of adhesion molecules ICAM-1 and VCAM-1 in the lung was also inhibited by **7w** and **7x** administration, which may partly explain the reduction of neutrophil infiltration. ALI is also characterized by hyperinflammation and the increased

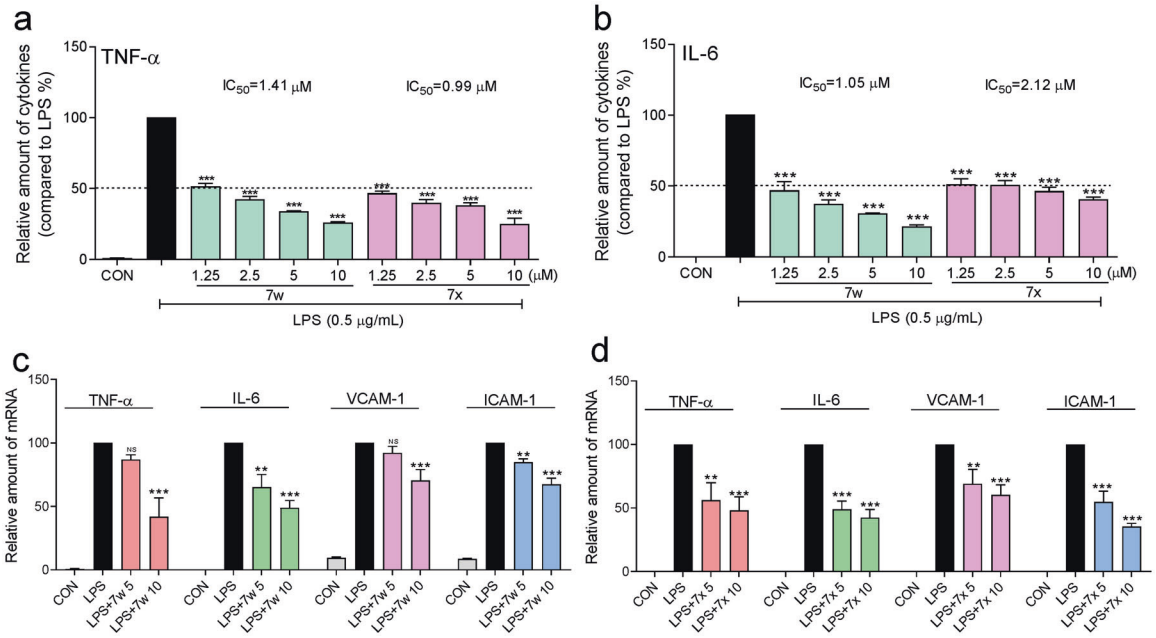

Fig. 3 7w and 7x inhibited LPS-induced inflammatory cytokine expression in macrophages. J774a.1 macrophages were pretreated with **7w** or **7x** at 1.25, 2.5, 5, or 10 μM for 30 min and then treated with LPS at 0.5 μg/mL for 24 h. DMSO was used as vehicle control. **a** TNF-α and **b** IL-6 levels in the medium were determined by ELISA. Data were normalized to total protein concentration from the same plate. For the detection of mRNA levels, MPMs were pretreated with vehicle control (DMSO), **7w** (5 or 10 μM) or **7x** (5 or 10 μM) for 30 min followed by incubation with LPS at 0.5 μg/ml for 6 h. **c**, **d** The mRNA levels of inflammatory cytokines TNF-α, IL-6, VCAM-1, and ICAM-1 were determined by RT-qPCR and normalized by β-actin mRNA level. Data were mean ± SEM of 3–5 independent experiments. $^{*}P < 0.05$, $^{**}P < 0.01$, $^{***}P < 0.001$ compared with LPS group.

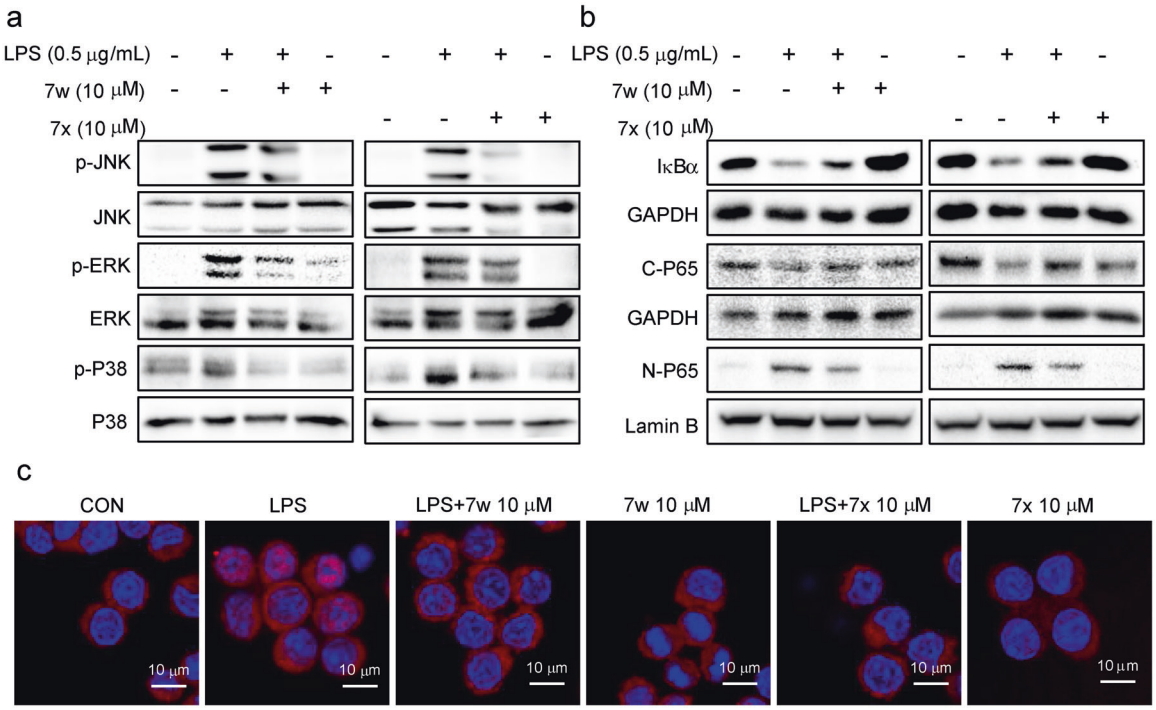

Fig. 4 7w and 7x suppressed LPS-induced MAPK phosphorylation and NF-κB activation in macrophages. a MPMs were pretreated with **7w** or **7x** at 10 μM for 30 min followed by incubation with LPS (0.5 μg/mL) for 30 min. The levels of p-JNK, p-ERK, and p-P38 were measured by Western blot. The corresponding total protein was the loading control. **b** MPMs were pretreated with **7w** (10 μM) or **7x** (10 μM) for 30 min, then were stimulated by LPS (0.5 μg/mL) for 45 min. IκBα, cytosolic, and nuclear P65 levels were detected by Western blot. GAPDH and lamin B were used as loading controls. **c** Immunofluorescent staining detected the nuclear translocation of P65 in MPMs (red: P65 positive stain; blue: nuclei positive stain).

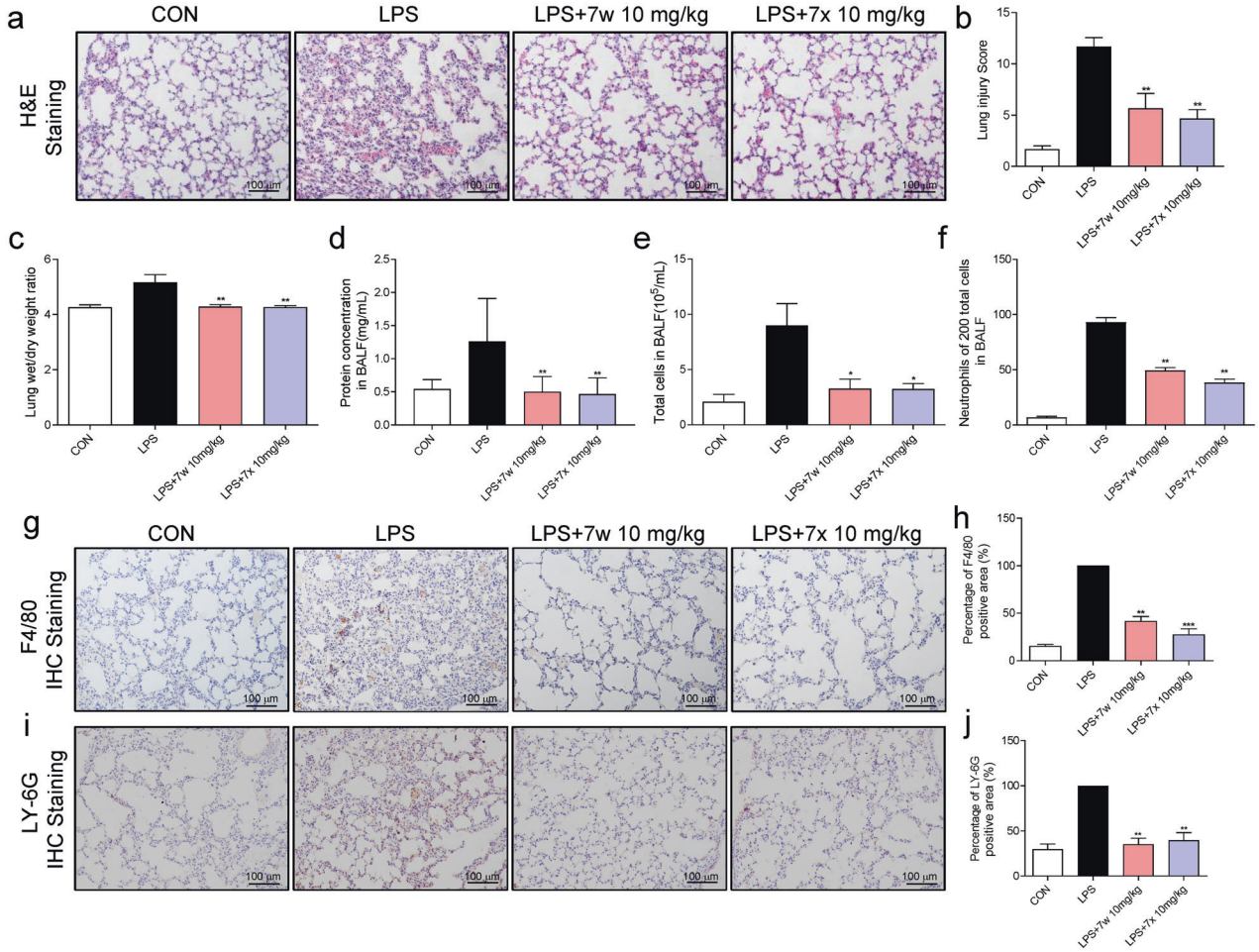

Fig. 5 7w and 7x prevented LPS-induced ALI in mice. C57BL/6 mice were pretreated with 10 mg/kg **7w** or **7x** via oral administration for 7 days, followed by intracheal injection of 5 mg/kg LPS, and lung samples were obtained 6 h later. **a** Representative H&E staining images of the lung. **b** Lung injury score as assessed by histological analysis of lung tissues. **c** The lung wet/dry weight ratio. **d** Total protein concentration in BALF. **e** Total cells in BALF. **f** The number of neutrophils in 200 total cells in BALF. **g**, **h** Representative images of immunohistochemical staining (brown) for macrophages (anti-F4/80) in lung tissues. **i**, **j** Representative images of immunohistochemical staining (brown) for neutrophils (anti-LY-6G) in lung tissues. Data were reported as mean ± SEM. $^*P < 0.05$, $^{**}P < 0.01$, $^{***}P < 0.001$ compared with LPS group; $n \geq 6$.

permeability of the alveolar-capillary barrier, which were similarly observed in the current LPS-induced ALI model [1]. According to our results, **7w** and **7x** administration played significantly role in reducing protein concentration and total cell counts in BALF post LPS challenge. Besides, the levels of pro-inflammatory cytokines TNF-α and IL-6 in serum, BALF and lung tissue were reduced as well. These results indicate that **7w** and **7x** have the potential for the treatment of ALI.

MD2 plays a pivotal role in recognition of LPS by TLR4 and the subsequent stimulation of MAPKs and NF-κB signaling pathway. MAPKs and NF-κB are the representative signaling pathways downstream of LPS-TLR4 pathway and have attracted plenty of attention as the primary anti-inflammatory mechanisms of drugs [13]. In response to LPS stimulation, MAPKs (ERK, JNK, and P38) are activated via phosphorylation, thus triggering cytokines release [26]. As suggested by our results, **7w** and **7x** pretreatment significantly inhibited LPS-induced phosphorylation of ERK, JNK and P38 in MPMs. In normal cells, NF-κB interacts with IκBα in cytoplasm to produce an inactive complex [27]. Upon stimulation, such as pathogen, cytokines and LPS, IκBα was phosphorylated and then degraded by ubiquitination, which leads to the active subunit NF-κB P65 transfer from the cytosolic to the nuclear fractions, then triggers inflammatory gene expression [27]. In this study, **7w** and **7x** evidently reversed LPS-induced IκBα degradation and nuclear translocation of P65 as revealed at the protein level in MPMs. These results suggest that **7w** and **7x** inhibit MAPKs and NF-κB activation by targeting MD2.

Recent studies have shown that MD2 inhibitors can attenuate LPS-induced inflammatory response both in vitro and in vivo. We noted that eritoran, a LPS-like MD2/TLR4 inhibitor, failed in the phase III clinical trial in the treatment of severe sepsis, due to the low efficiency [28]. The high interaction between Eritoran and serum proteins reduces its clinic pharmacokinetics and results in low effectiveness. However, we believe that small-molecule MD2 inhibitors, which tolerate the serum proteins, could be a better choice for the treatment of sepsis. Although no compounds inhibiting MD2 have entered clinical trials, developing non-lipid MD2 inhibitors could be a potential strategy. Previous studies already identified several compounds derived from natural products and their analogs that can directly bind to MD2 and exhibit anti-inflammatory activities [15, 16, 19, 20]. Herein, it was demonstrated that compounds **7w** and **7x** directly bound to rhMD2 protein with the K_D values of 96.2 μM and 31.2 μM, respectively. Although LPS has higher binding affinity to MD2, compounds **7w** and **7x**, at a much higher concentration (5 or 10 μM) than LPS (0.5 μg/mL), significantly antagonized LPS binding to MD2 in both cell-free system and cultured macrophages (Figs. 2–4). Interestingly, the binding affinities of **7w** and **7x** to rhMD2 were

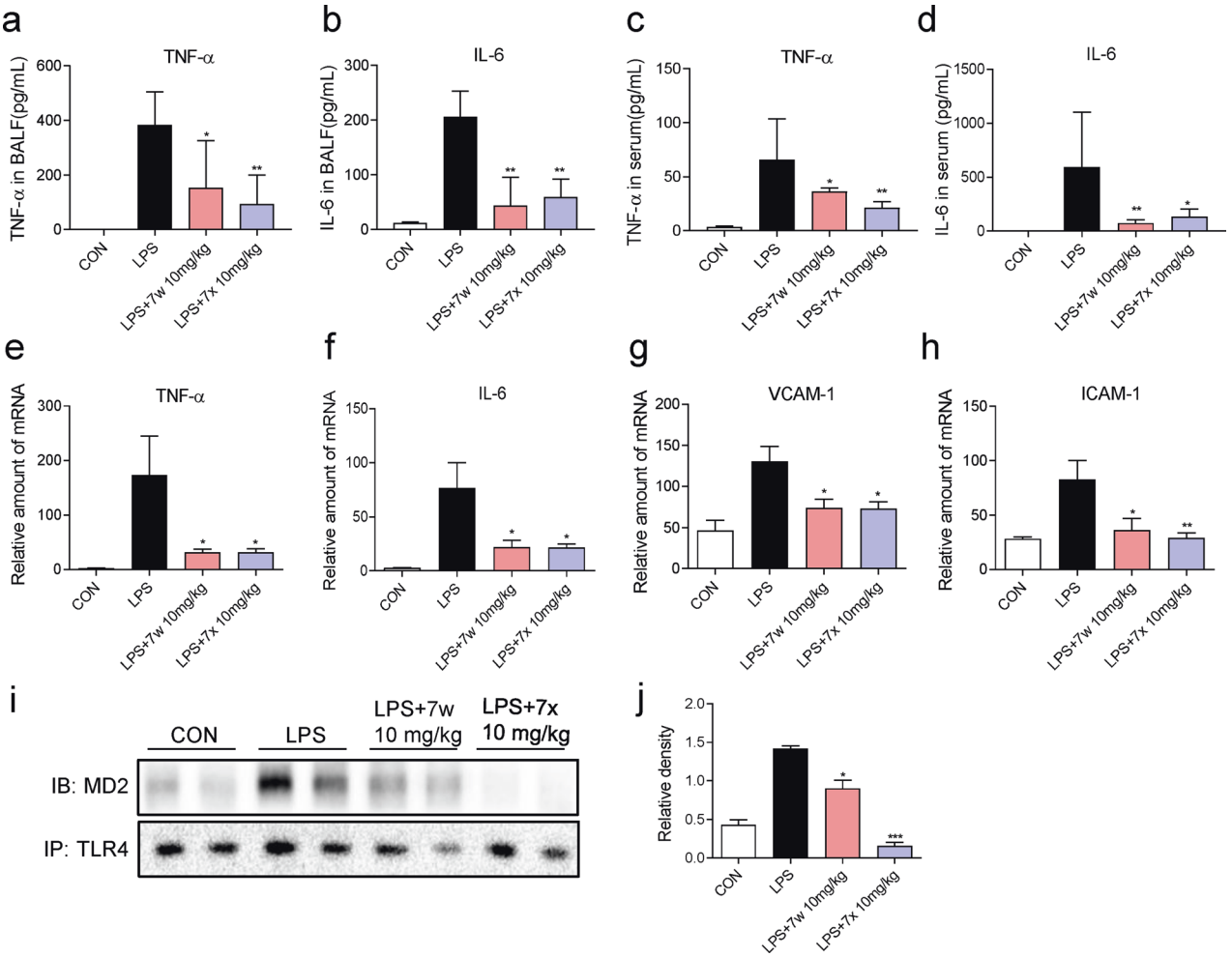

Fig. 6 7w and 7x inhibited LPS-induced lung inflammation in mice by targeting MD2. C57BL/6 mice were pretreated with 10 mg/kg **7w** or **7x** via oral administration for 7 days, followed by intracheal injection of 5 mg/kg LPS, and lung samples were obtained 6 h later. **a**, **c** TNF-α and **b**, **d** IL-6 in BALF and serum from the experimental mice were determined with ELISA. **e**–**h** The mRNA levels of inflammatory cytokines in the lung tissues were determined by RT-qPCR after LPS treatment. Cytokine gene expression was normalized to β-actin. **i 7w** and **7x** inhibited the formation of MD2-TLR4 complex in the lung tissues. **j** Densitometric quantification of blot in **i**. Data were reported as mean ± SEM. $^{*}P < 0.05$, $^{**}P < 0.01$, $^{***}P < 0.001$ compared with LPS group; $n \geq 6$.

higher when compared to other known MD2 inhibitors, such as compound **20** (K_D: 189 μM) and xanthohumal (K_D: 460 μM) [17, 19]. Compound **7x** also showed a lower K_D value as compared to other MD2 inhibitors, including L6H21 (33.3 μM), L6H9 (31.6 μM), and baicalein (79.5 μM) [15, 18, 29]. We also note that **7w** and **7x** could not dose-dependently and completely block the interaction between LPS and rhMD2 (Fig. 2g), as MD2 protein has a big pocket and **7w**/**7x** only binds to a relatively small site of MD2 pocket (Fig. 2a, b). Therefore, a part of LPS lipid chains may still insert into the **7w**/**7x**-containing MD2 pocket. However, the **7w**/**7x**-MD2 interaction obviously influences the quality of LPS-MD2 binding and prevents LPS to activate a right conformation of MD2 for MD2 activation, evidenced by the fact that **7w**/**7x** at 10 μM completely blocked LPS induced MD2-TLR4 interaction (Fig. 1h, i). These results indicate that **7w** and **7x** may be more effective MD2 inhibitors, which is the novelty of this work. Of course, further experiments for **7w**/**7x**-based drug design and development are needed.

MD2 activation also participates in the pathogenesis of various chronic inflammatory diseases and cancers, such as diabetic cardiomyopathy, atherosclerosis, asthma, and colon cancer [30–33]. In our previous studies, we have shown that MD2 is a direct receptor of palmitic acid and AGEs, driving inflammatory response in metabolic heart diseases [29, 33]. Pharmacological or genetic MD2 inhibition has shown to hinder the progression of these diseases. As MD2 inhibitors, we consider that **7w** and **7x** are also able to block MD2-mediated inflammation induced by DAMPs (e.g., AGEs in Supplementary Fig. S3), which enables **7w** and **7x** have therapeutic potential not only for LPS-related acute inflammatory diseases but also for other chronic metabolic diseases. This is certainly a focus of future studies.

A limitation of this study may be the absence of a positive control (clinical drug). However, there is no effective drug used in the treatment of ALI in clinic so far. The mostly used drugs are glucocorticoids, which has totally different mechanism compared to **7w** and **7x**. In addition, as the steroidal anti-inflammatory drugs, glucocorticoids exhibit many side-effects, including Cushing's syndrome and osteoporosis. Here, we demonstrated that targeting MD2 by compounds **7w** and **7x** inhibited the formation of LPS-MD2-TLR4 complex, and consequently, downstream signaling pathway activation and inflammatory injuries. These data indicates that MD2 inhibition may be a better strategy than glucocorticoids for the treatment of ALI. We will compare the MD2 inhibitors with glucocorticoids in the future evaluations.

In conclusion, compounds **7w** and **7x** were identified as the novel MD2 inhibitors that can inhibit inflammatory response both

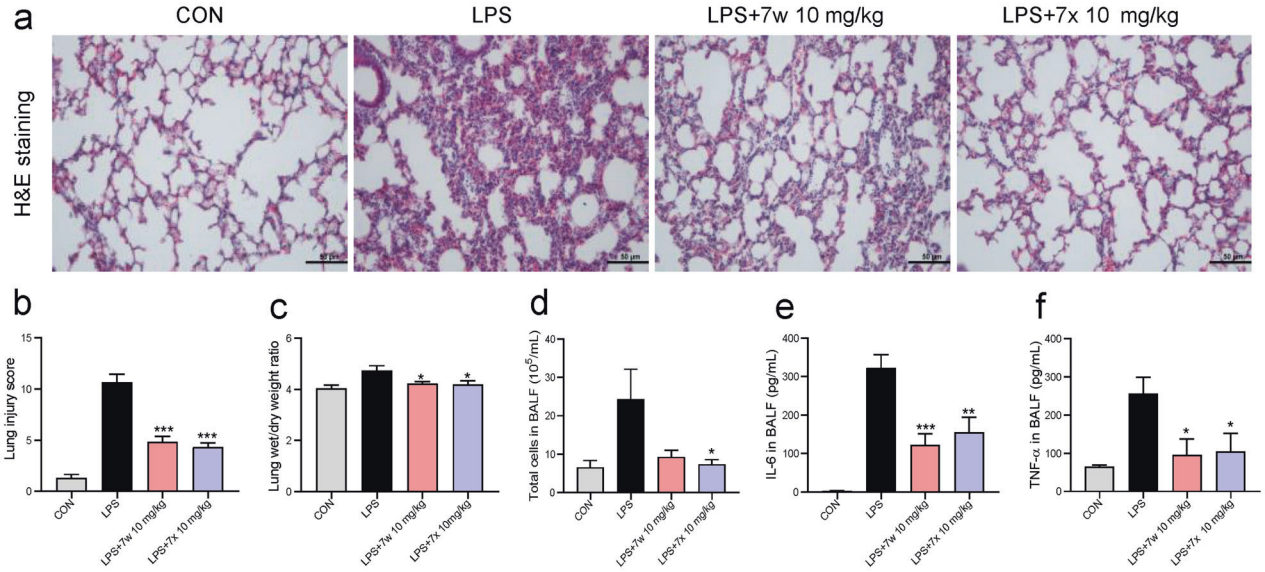

Fig. 7 Compounds 7w and 7x showed therapeutic effects in mice with LPS-induced ALI. C57BL/6 mice were intragastricly administered 10 mg/kg **7w** or **7x** 1 h after intratracheal injection of 5 mg/kg LPS. Lung tissues and BALF were collected 6 h after LPS injection. **a** Representative H&E staining images of the lung. **b** Lung injury score as assessed by histological analysis of lung tissues. **c** The lung wet/dry weight ratio. **d** Total cells in BALF. The levels of IL-6 (**e**) and TNF-α (**f**) in BALF from the experimental mice were determined with ELISA. Data are reported as mean ± SEM, $n \geq 6$ per group. $^{*}P < 0.05$, $^{**}P < 0.01$, $^{***}P < 0.001$ compared with LPS group.

in vitro and in vivo. These data demonstrate the therapeutic potential of **7w** and **7x** for the treatment of ALI and other inflammatory diseases.

ACKNOWLEDGEMENTS

This study was supported by the National Key Research and Development Project (2019ZX09301-148), National Natural Science Foundation of China (81872918, 81970323, 81973168, and 21961142009), Thailand Research Fund Grant (DBG6280006), Zhejiang Key Research and Development Project (2018C03068), Wenzhou Key Research and Development Project (2018ZY009) and Zhejiang College Student's Science and Technology Innovation Activities Program (2021R413015).

AUTHOR CONTRIBUTIONS

YLZ, JQY, WXZ, WJJ, YLT, and ZWX collected, analyzed and interpreted data; GL, YLZ, and ZGL designed experiments, interpreted the data, and wrote the manuscript; YW, NC, MJX, and JPF revised the manuscript.

ADDITIONAL INFORMATION

Supplementary information The online version contains supplementary material available at https://doi.org/10.1038/s41401-021-00764-8.

Competing interests: The authors declare no competing interests.

REFERENCES

1. Matthay M, Zemans R, Zimmerman G, Arabi Y, Beitler J, Mercat A, et al. Acute respiratory distress syndrome. Nat Rev Dis Prim. 2019;5:18.
2. Rubenfeld G, Caldwell E, Peabody E, Weaver J, Martin D, Neff M, et al. Incidence and outcomes of acute lung injury. N Engl J Med. 2005;353:1685–93.
3. Slutsky A. History of mechanical ventilation. From vesalius to ventilator-induced lung injury. Am J Respir Crit Care Med. 2015;191:1106–15.
4. Wohlauer M, Moore E, Silliman C, Fragoso M, Gamboni F, Harr J, et al. Nebulized hypertonic saline attenuates acute lung injury following trauma and hemorrhagic shock via inhibition of matrix metalloproteinase-13. Crit Care Med. 2012;40:2647–53.
5. Cheng K, Xiong S, Ye Z, Hong Z, Di A, Tsang K, et al. Caspase-11-mediated endothelial pyroptosis underlies endotoxemia-induced lung injury. J Clin Invest. 2017;127:4124–35.
6. Wang W, Pei X, Xu M, Sun S, Zhang C, Mu K, et al. The protective effect of sodium ferulate and oxymatrine combination on paraquat-induced lung injury. Iran J Pharm Res. 2015;14:573–83.
7. Bellani G, Laffey J, Pham T, Fan E, Brochard L, Esteban A, et al. Epidemiology, patterns of care, and mortality for patients with acute respiratory distress syndrome in intensive care units in 50 Countries. JAMA. 2016;315:788–800.
8. Pham T, Rubenfeld G. Fifty years of research in ARDS. The rpidemiology of acute respiratory distress syndrome. A 50th birthday review. Am J Respir Crit Care Med. 2017;195:860–70.
9. Sercundes M, Ortolan L, Debone D, Soeiro-Pereira P, Gomes E, Aitken E, et al. Targeting neutrophils to prevent malaria-associated acute lung injury/acute respiratory distress syndrome in mice. PLoS Pathog. 2016;12:e1006054.
10. Gao Y, Jiang W, Dong C, Li C, Fu X, Min L, et al. Anti-inflammatory effects of sophocarpine in LPS-induced RAW 264.7 cells via NF-κB and MAPKs signaling pathways. Toxicol Vitr. 2012;26:1–6.
11. Rojas M, Woods C, Mora A, Xu J, Brigham K. Endotoxin-induced lung injury in mice: structural, functional, and biochemical responses. Am J Physiol Lung Cell Mol Physiol. 2005;288:L333–41.
12. Beom Seok P, Hyun SD, Ho Min K, Byong-Seok C, Hayyoung L, Jie-Oh L. The structural basis of lipopolysaccharide recognition by the TLR4-MD-2 complex. Nature. 2009;458:1191–5.
13. Akira S, Takeda K. Toll-like receptor signalling. Nat Rev Immunol. 2004;4:499–511.
14. Fitzgerald K, Kagan J. Toll-like receptors and the control of immunity. Cell. 2020;180:1044–66.
15. Chen H, Zhang Y, Zhang W, Liu H, Sun C, Zhang B, et al. Inhibition of myeloid differentiation factor 2 by baicalein protects against acute lung injury. Phytomedicine. 2019;63:152997.
16. Zhang Y, Xu T, Pan Z, Ge X, Sun C, Lu C, et al. Shikonin inhibits myeloid differentiation protein 2 to prevent LPS-induced acute lung injury. Br J Pharmacol. 2018;175:840–54.
17. Fu W, Chen L, Wang Z, Zhao C, Chen G, Liu X, et al. Determination of the binding mode for anti-inflammatory natural product xanthohumol with myeloid differentiation protein 2. Drug Des Devel Ther. 2016;10:455–63.
18. Wang Y, Shan X, Chen G, Jiang L, Wang Z, Fang Q, et al. MD-2 as the target of a novel small molecule, L6H21, in the attenuation of LPS-induced inflammatory response and sepsis. Br J Pharmacol. 2015;172:4391–405.
19. Zhang Y, Wu J, Ying S, Chen G, Wu B, Xu T, et al. Discovery of new MD2 inhibitor from chalcone derivatives with anti-inflammatory effects in LPS-induced acute lung injury. Sci Rep. 2016;6:25130.
20. Zhang Y, Xu T, Wu B, Chen H, Pan Z, Huang Y, et al. Targeting myeloid differentiation protein 2 by the new chalcone L2H21 protects LPS-induced acute lung injury. J Cell Mol Med. 2017;21:746–57.

21. Xiao S, Zhang W, Chen H, Fang B, Qiu Y, Chen X, et al. Design, synthesis, and structure-activity relationships of 2-benzylidene-1-indanone derivatives as anti-inflammatory agents for treatment of acute lung injury. Drug Des Devel Ther. 2018;12:887–99.
22. Grommes J, Soehnlein O. Contribution of neutrophils to acute lung injury. Mol Med. 2011;17:293–307.
23. Wessels I, Pupke J, Von Trotha K, Gombert A, Himmelsbach A, Fischer H, et al. Zinc supplementation ameliorates lung injury by reducing neutrophil recruitment and activity. Thorax. 2020;75:253–61.
24. Aggarwal A, Baker CS, Evans TW, Haslam PL. G-CSF and IL-8 but not GM-CSF correlate with severity of pulmonary neutrophilia in acute respiratory distress syndrome. Eur Respir J. 2000;15:895–901.
25. Németh T, Sperandio M, Mócsai A. Neutrophils as emerging therapeutic targets. Nat Rev Drug Discov. 2020;19:253–75.
26. Kim EK, Choi EJ. Pathological roles of MAPK signaling pathways in human diseases. Biochim Biophys Acta Mol Basis Dis. 2010;1802:396–405.
27. Adli M, Merkhofer E, Cogswell P, Baldwin A. IKKalpha and IKKbeta each function to regulate NF-kappaB activation in the TNF-induced/canonical pathway. PLoS One. 2010;5:e9428.
28. Opal S, Laterre P, Francois B, Larosa S, Angus D, Mira J, et al. Effect of eritoran, an antagonist of MD2-TLR4, on mortality in patients with severe sepsis: the ACCESS randomized trial. JAMA. 2013;309:1154–62.
29. Wang Y, Qian Y, Fang Q, Zhong P, Li W, Wang L, et al. Saturated palmitic acid induces myocardial inflammatory injuries through direct binding to TLR4 accessory protein MD2. Nat Commun. 2017;8:13997.
30. Chen T, Huang W, Qian J, Luo W, Shan P, Cai Y, et al. Macrophage-derived myeloid differentiation protein 2 plays an essential role in ox-LDL-induced inflammation and atherosclerosis. EBioMedicine. 2020;53:102706.
31. Hosoki K, Boldogh I, Aguilera-Aguirre L, Sun Q, Itazawa T, Hazra T, et al. Myeloid differentiation protein 2 facilitates pollen- and cat dander-induced innate and allergic airway inflammation. J Allergy Clin Immunol. 2016; 137:1506–.e2.
32. Rajamanickam V, Yan T, Xu S, Hui J, Xu X, Ren L, et al. Selective targeting of the TLR4 co-receptor, MD2, prevents colon cancer growth and lung metastasis. Int J Biol Sci. 2020;16:1288–302.
33. Wang Y, Luo W, Han J, Khan Z, Fang Q, Jin Y, et al. MD2 activation by direct AGE interaction drives inflammatory diabetic cardiomyopathy. Nat Commun. 2020;11:2148.